

## Toward a physical model of the clavichord

Jean-Théo Jiolat, Christophe d'Alessandro, Jean-Loïc Le Carrou, et al.

Citation: *The Journal of the Acoustical Society of America* **150**, 2350 (2021); doi: 10.1121/10.0006438

View online: <https://doi.org/10.1121/10.0006438>

View Table of Contents: <https://asa.scitation.org/toc/jas/150/4>

Published by the *Acoustical Society of America*

---

---



**Advance your science and career  
as a member of the**

**ACOUSTICAL SOCIETY OF AMERICA**

LEARN MORE



## Toward a physical model of the clavichord<sup>a)</sup>

Jean-Théo Jiolat,<sup>1</sup> Christophe d'Alessandro,<sup>1,b)</sup> Jean-Loïc Le Carrou,<sup>1</sup> and José Antunes<sup>2,c)</sup>

<sup>1</sup>*Institut Jean Le Rond d'Alembert, Équipe Lutheries-Acoustique-Musique, Sorbonne Université, CNRS, F-75005 Paris, France*

<sup>2</sup>*Applied Dynamics Laboratory, Instituto Superior Técnico, Centro de Ciências e Tecnologias Nucleares, Bobadela, Portugal*

### ABSTRACT:

String excitation by the tangent in the clavichord is a unique mechanism. The tangent, keeping in contact with the string after the initial strike, continuously controls the string tension. Four main flexible subsystems are considered in the clavichord: the tangent/key subsystem, the string subsystem, the bridge-soundboard subsystem, and the string damper subsystem. A modal description of the dynamics of these subsystems is proposed. Parameters of the subsystems are estimated on a copy of a historical instrument by Hubert (1784). The different subsystems and their couplings are modeled using a modal Udewadia–Kalaba formulation. The string-tangent interaction is modeled via the intermittent contact dynamics, using the Kirchoff–Carrier string model. Realistic string, soundboard, and tangent motions are obtained using a time-domain synthesis scheme that computes the dynamics of the uncoupled subsystems and the constraints resulting from coupling between them. Simulated motions of the model in response to a driving force on the key are analyzed. The results are consistent with experimental measurements and published data on the dynamics of the clavichord. The model is able to reproduce the main acoustic features of the instrument: force on the key for intonation control, key velocity for dynamic nuances control, and constant spectral slope for varying dynamic nuances. © 2021 Acoustical Society of America. <https://doi.org/10.1121/10.0006438>

(Received 11 February 2021; revised 14 August 2021; accepted 19 August 2021; published online 4 October 2021)

[Editor: Vasileios Chatziioannou]

Pages: 2350–2363

### I. INTRODUCTION

The clavichord is highly prized as a practice instrument among keyboard players because of its superior ability to encourage a polished technique.<sup>1</sup> Its sound is weak and sometimes a little disappointing upon first contact with the instrument. One explanation for the special appreciation of the clavichord as a wonderful coach of finger technique lies in the refined string control allowed by its simple and direct action. In the clavichord, the string and tangent stay in contact, i.e., are mechanically coupled, as long as the key remains depressed (see Ref. 2 for a thorough presentation of the instrument). This feature has important consequences for the sound and the dynamic of the instrument, allowing for expressive pitch control, a unique feature among stringed keyboard instruments. The aim of the present research is to develop a physical model of the clavichord that is able to account for and synthesize the specific feature of the clavichord's action, from finger motion to soundboard vibration.

Relatively few acoustic studies on the clavichord have been published so far. The first ones<sup>3,4</sup> mainly report descriptions of sound features (level, spectrum) due to the tangent action compared to the piano and harpsichord actions. A study on the clavichord touch and action is developed in Ref. 5, showing that hardness of touch and pitch stability are related to string tension and key balance

parameters. Some aspects of the physics of the instrument are investigated in Ref. 6: soundboard and cavity coupling, tangent velocity profile and string displacement, sound decay rate, and string pair coupling effects. A linear string model is used for qualitative explanation of the tangent velocity profile (modeled as an exponential decaying function), string motion, and sound decay rate. Based on these results, a comparison with the piano and harpsichord is derived in Ref. 7. Focusing on the string excitation mechanism, the dynamics of the clavichord is revisited in Ref. 8. A mass-spring-damper model of the key/tangent and string system oscillation is developed. Using a quasi-static approximation of the string motion and a delay-line model of the string, the excitation dynamics is studied and compared to experimental data. A linear relationship between tangent velocity and sound pressure level (SPL) is found. String displacement (and then variation of string tension) has a significant effect on fundamental frequency, but the sound spectral slope does not vary much with tangent velocity or displacement. Measurements on four clavichords are in good agreement with these findings.<sup>9</sup> Musical consequences of the needed joint tangent displacement/velocity controls for the clavichord playing technique are studied in terms of the so-called “clavichord's paradox.”<sup>10</sup>

As for sound synthesis, two approaches for physical modeling of the clavichord have been published so far. The signal processing approach in Ref. 11 is based on commuted wave-guide synthesis: string/tangent interaction is partly based on sampling of real sounds (for a realistic knock sound) and partly on additional filters accounting for the

<sup>a)</sup>This paper is part of a special issue on Modeling of Musical Instruments.

<sup>b)</sup>ORCID: 0000-0002-2629-8752.

<sup>c)</sup>Also at Instituto de Etnomusicologia, Centro de Estudos em Música e Dança, Universidade Nova de Lisboa, Lisbon, Portugal.

variable string tension during a tone. Physical modeling of the piano gave birth to a successful software piano synthesizer able to produce realistic sound synthesis for modern and historical pianos, for harpsichords as well as for hybrid instruments, and for the clavichord.<sup>12</sup> For commercial reasons, the physical modeling techniques used and specific features for the clavichord model are not published, but it seems that a hard metallic hammer is simulated for the initial tangent strike, together with an additional after-touch effect accounting for the enforced tangent/string contact. Note that other physical piano models based on finite element techniques have been developed and published.<sup>13,14</sup>

The aim of this paper is to develop a physical model of the clavichord with special attention to the collision and contact between the tangent and the string, which is of prime importance for explaining the instrument's dynamics and sound features. Intermittent contacts are often encountered in musical instruments and have been studied in numerous works in the past decade. Collisions (see Ref. 15 for a review on the subject) are modeled by a penalty approach;<sup>16,17</sup> by nonsmooth contact dynamics, which is particularly adapted for hard contacts<sup>18</sup> or dry-friction and stick-slip transitions;<sup>19</sup> or by a Lagrange multiplier approach, particularly fit for multibody systems.<sup>20</sup> This last method coupled to the modal Udewadia–Kalaba (U–K) formulation seemed appropriate for the clavichord, following recent results for stringed instruments,<sup>21</sup> including the guitar

and Portuguese guitar.<sup>22,23</sup> In Sec. II, a functional description of the clavichord in terms of vibrating subsystems results in a simplified one-string model. Parameters are identified using experimental measurements on a copy of a historical instrument. A model of tangent/string interaction based on the Kirchhoff–Carrier string representation and the U–K formulation for coupled dynamical systems is developed for the one-string clavichord model in Sec. III. The modal equations of the U–K model can be solved by means of a simple finite difference time discretization scheme. Synthesis results are compared to the measured dynamic behavior of the real clavichord using experiments and published data in Sec. IV.

## II. VIBRATORY AND ACOUSTIC SUBSYSTEMS IN THE CLAVICHORD

### A. Principle of the clavichord and tangent action

A clavichord and its parts are described in Fig. 1(a) [instrument built in 2007 and inspired by a Hubert (1784) historical model]. The main parts of the instrument are indicated on the picture. The strings, organized in pairs, are stretched between the hitch-pins and tuning pins and attached to the radiating soundboard through the bridge and bridge pin. Strings are functionally divided into three sections. The “damped section” is between the hitch-pin and the tangent. This section is partially covered by strips of

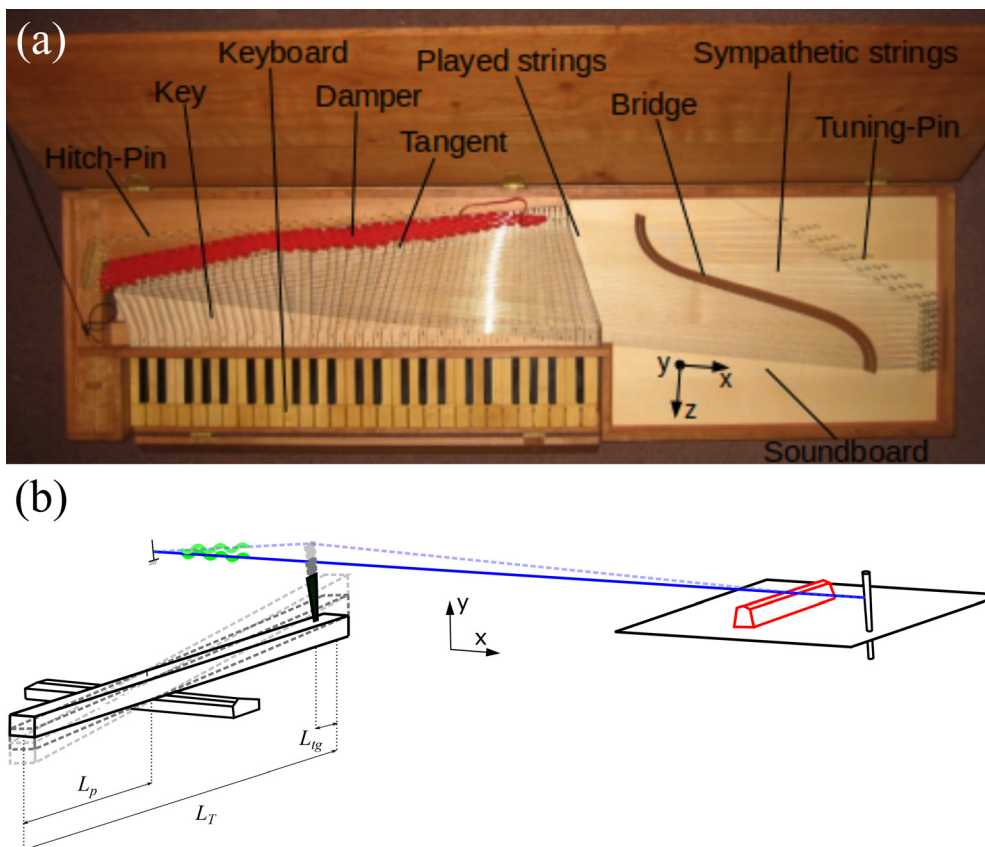


FIG. 1. (Color online) (a) Description of a clavichord; (b) sketch of the clavichord's mechanism in three positions of the touch: at rest, the tangent flushing the string, and after excitation.

cloth. Its vibration is rapidly damped after excitation. The “played section” vibrates between the tangent and bridge as long as the tangent stays in contact with the string after the initial tangent strike. When the key is released, the tangent contact is lost, and the string vibration is damped by the cloth strips. The “resting section,” between the bridge and the tuning pin, is not directly excited by the tangent, but as it is not damped in the clavichord (contrary to, e.g., the square piano), partial transmission of the played section vibration results in sympathetic vibration.<sup>24,25</sup> The strings are pressed vertically on the bridge and pressed horizontally on the bridge pins laid out along the bridge. This contact leads to the soundboard/string coupling. The soundboard vibrates under the action of the string, and because of its large surface, sound is radiated in the air.

A complete study of the instrument is beyond the scope of the present work: only the simplified model displayed in Fig. 1(b) is studied in depth. This simplified model is made of only one string (the chosen string is the first string of the G#<sub>3</sub> choir) and the corresponding key, tangent, and damper. The string is stretched between the hitch-pin and tuning pin and in contact with the bridge at the bridge pin. The soundboard and bridge are those of the whole instrument because it is important to consider this part in its integrity even for modeling a unique string. Other aspects of the instrument, like the case and lid, are not considered in the present study, because their vibratory and acoustic functions are only of second order.

**B. Vibratory and acoustic subsystems**

For modeling purposes, the model can be considered as an assembly of four vibrating subsystems as displayed in Fig. 2. The initial force for playing the instrument is provided by the player’s finger. The player moves the tangent/key subsystem, the first subsystem, providing the string

excitation. The strings, the second subsystem, act as the vibratory engine of the instrument. Attached to the left side of the strings are the cloth dampers, the third subsystem. Attached to the right side of the strings is the bridge/soundboard subsystem, the fourth subsystem.

The string is the central subsystem of the instrument. Let  $Y^S(x, t)$  [respectively,  $Y^D(x, t)$ ,  $Y^k(x, t)$ ,  $Y^B(x_B, t)$ ] be the string displacement (respectively, damper displacement, key-tangent subsystem displacement, bridge displacement) at position  $x$  (respectively,  $x$ ,  $x$ ,  $x_B$ ). The vibratory subsystems are coupled to the string at points  $x_{Di}$ ,  $x_{Ltg}$ ,  $x_B$  ( $i$ th damper, tangent, and bridge). The first subsystem, the tangent/key subsystem, can be considered as a rigid rod that tilts with respect to a pivot. When the tangent strikes the string, the elastic string reacts and the whole system oscillates. The tangent has a mass  $M_{Tg} = 5$  g, and the key has a mass  $M_k = 30$  g. The length of the key is  $L_T = 28.9$  cm. The pivot of the key (balance point) is situated at a distance  $L_p = 17.2$  cm of the back of the key, the finger presses the key at a distance  $L_f = 27.9$  cm of the back of the key, and the tangent is located at a distance  $L_{tg} = 3.5$  cm of the back of the key [see Fig. 1(b)]. Associated modal parameters for the tangent/key subsystem ( $k^k$ ,  $m^k$ ,  $c^k$ ) are used. The string, the second subsystem, is characterized by its mass, elasticity, and damping factors. Between the hitch-pin and excitation point, the third subsystem is the cloth strips damper, represented by  $N$  parallel dash-pots characterized by their mass and viscous damping coefficients ( $m^D$ ,  $c^D$ ). The number of dampers is set empirically to  $N = 65$ , as it seemed enough to ensure effective damping.

In the remainder of Sec. II, parameters of the subsystems in Fig. 2 are estimated using the instrument displayed in Fig. 1(a) and the G#<sub>3</sub> string. Three functional parts of the string can be identified: between  $x = 0$  m and  $x = 0.2$  m is the damped part of the string, with a cloth damper coiled up

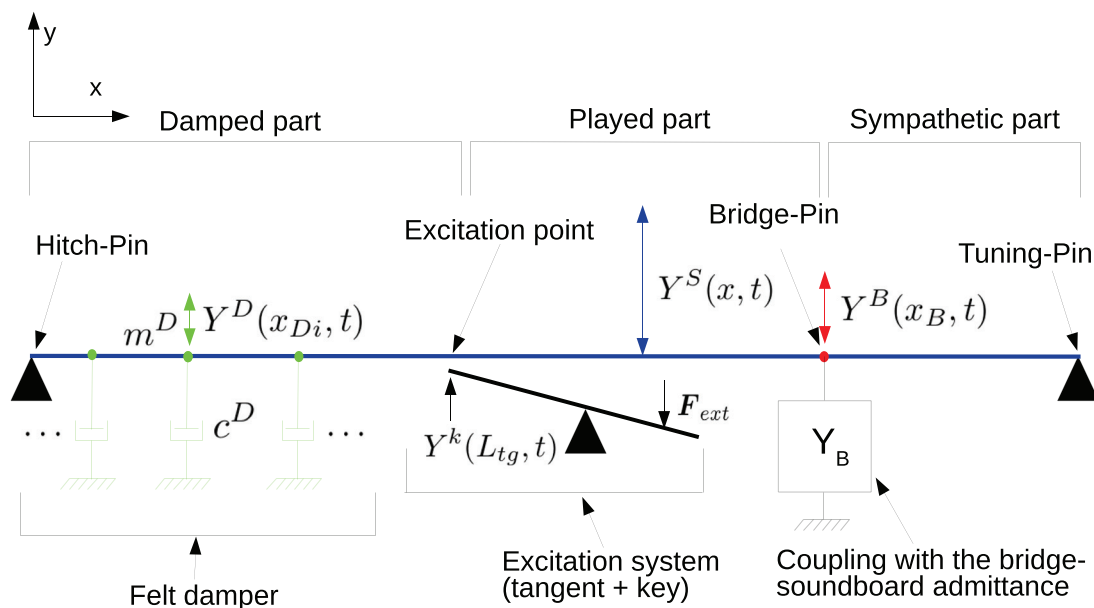


FIG. 2. (Color online) Schema of the modeled G#<sub>3</sub> string being excited by the tangent.

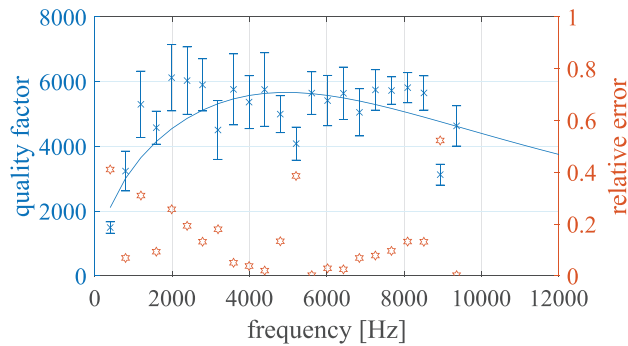


FIG. 3. (Color online) String quality factor: experimental (blue cross) and theoretical (blue line) with 95% error bars (blue) and relative error (red stars).

between  $x = 3.4$  cm and  $x = 13.7$  cm. The played part of the string is between  $x = 0.2$  m and  $x = 0.53$  m. The sympathetic part of the string is between the bridge pin  $x = 0.53$  m and tuning pin  $x = 0.84$  m.

**C. The key-tangent subsystem**

The key-tangent subsystem mass (determined in Sec. III B) is  $m^k = 1.17 \times 10^{-2}$  kg. It is represented by a rigid body mode, and its stiffness is  $k^k = 0$  N m<sup>-1</sup>. Its damping is set to  $c^k = 2.5$  kg·s<sup>-1</sup> to reproduce the low frequency oscillation damping of the tangent-string contact point observed in Sec. IV B.

**D. The string subsystem**

The string modal damping characteristics are obtained by measurements of the vibrating string stretched on a string sand bench, allowing for measurements with almost full decoupling of the string from other vibratory structures. The Valette and Cuesta string model (see Sec. III C 3) is used. The string is excited by a copper wire that breaks at a given tension when lifted vertically. The vibratory displacement of the string is measured at the other extremity by means of optical forks.<sup>26</sup> For the right (sympathetic) part of the G#<sub>3</sub> string ( $L = 31.7$  cm,  $d_s = 0.33$  mm,  $f_0 = 396.9$  Hz), damping characteristics for 23 partials between 396.9 and 9354 Hz are analyzed using the high-resolution algorithm ESPRIT.<sup>27–29</sup>

The measured damping coefficients are matched with the Valette and Cuesta model and displayed in Fig. 3, with the parameters reported in Table I, where  $E$  and  $\rho$  correspond to the Young’s modulus and density of a brass string, respectively;  $\eta_{air}$  and  $\rho_{air}$  are taken from the previous data;<sup>30</sup> and other parameters are defined in Sec. III C 3.

TABLE I. String’s parameters used to simulate the string damping coefficients.

$\rho$ (kg m <sup>-3</sup> )	$E$ (Pa)	$\delta_{ve-te}$
7000	$80 \times 10^9$	$1.5 \times 10^{-4}$
$Q_{struc}$	$\eta_{air}$ (kg m <sup>-1</sup> s <sup>-1</sup> )	$\rho_{air}$ (kg m <sup>-3</sup> )
$2.5 \times 10^4$	$1.8 \times 10^{-5}$	1.2

Experimental  $Q_{exp}$  and theoretical  $Q_{th}$  quality factors are reported together with 95% error bars for ten measures and relative error  $\epsilon_Q = (|Q_{exp} - Q_{th}|)/Q_{exp}$ .

**E. Bridge and soundboard subsystems**

To simulate the vibratory motion of the bridge, the modal parameters (mass matrix, stiffness matrix, damping matrix, mode shapes) of this subsystem need to be known. As no analytical solutions can be given for such a system, modal parameters of the bridge are estimated by means of experimental modal analysis<sup>21</sup> based on measurements of the bridge frequency response function (FRF). The FRF is obtained by measurement of the vibratory response at the coupling point between the bridge and the G#<sub>3</sub> string [using a PCB (Depew, NY) M352C65 accelerometer and an acquisition system with a sample rate of 51.2 kHz and a 24-bit depth]. The system is excited by an automatic impact hammer (force sensor PCB 086E80). The accelerometer is placed above the bridge pin and measures its vertical acceleration. All the other strings are damped by strips of cloth woven on both sides of the strings (above the soundboard on the right side and above the keyboard on the left side). Modal analysis between 100 and 3500 Hz is conducted in two steps. The first step is the estimation of physical poles containing the modal frequencies and damping coefficients of the analyzed structure, using the least square rational function (LSRF) estimation method (MATLAB signal processing toolbox<sup>31</sup>). The second step is the estimation of residues that encapsulate the mode shapes and modal masses of the system. Normalizing modal masses to  $m_n = 1$  kg for modes  $n = 1, 2, \dots, N_B$ , and the corresponding mode shapes are estimated from the residues. The estimated and measured FRF at the G#<sub>3</sub> string/bridge coupling point are plotted on Fig. 4. Thirty-one bridge modes are identified between 100 and 600 Hz, giving a satisfying reconstruction of the FRF. One hundred eight bridge modes are identified between 600 and 3500 Hz, giving a representation of the bridge mobility for higher frequencies. High frequency modeling is necessary for a realistic simulation, even if it does not comply exactly to physical modes of the system, as previously discussed in Ref. 32. Measured and reconstructed impulse responses are given in sound examples Mm. 1 and Mm. 2, respectively.

Mm. 1. Measured impulse response at the G#<sub>3</sub> string/bridge coupling point. This is a file of type “wav” (601 KB).

Mm. 2. Reconstructed impulse response at the G#<sub>3</sub> string/bridge coupling point. This is a file of type “wav” (601 KB).

**F. The damper subsystem, coupling between subsystems and activation**

The felt damper is modeled by a series of 65 dash-pots. The parameters  $c^D$ ,  $m^D$  are chosen so that the measured damping effect exerted on the string once the key is released is

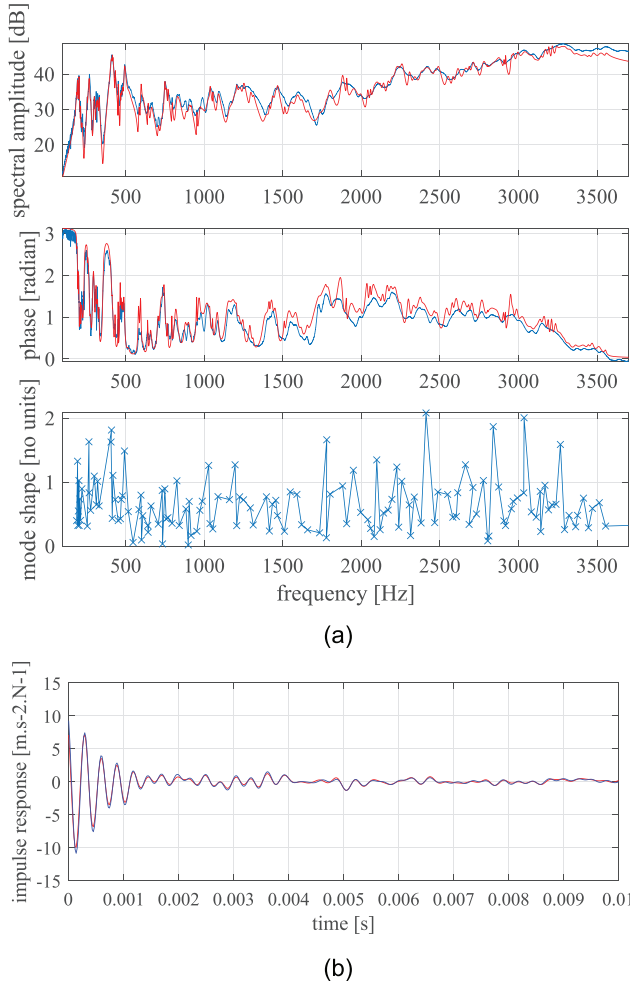


FIG. 4. (Color online) Bridge and soundboard modal analysis. (a) Top panel: comparison of the spectral magnitude (ref 1 dB: 1m s<sup>2</sup> N<sup>-1</sup>) of the measured (blue) and reconstructed (red) FRF. Middle panel: corresponding unwrapped phase. Bottom panel: corresponding mode shapes. (b) corresponding measured (blue) and reconstructed (red) impulse responses.

well reproduced. The values chosen are  $m^D = 1.0 \times 10^{-2}$  kg and  $c^D = 8.0 \times 10^2$  kg s<sup>-1</sup>.

The four subsystems are coupled through the string: the string is coupled to the damper at the damper location; it is coupled to the bridge at the bridge pin location; it is coupled to the tangent/key subsystem during its contact at the tangent location. All these coupling conditions assume a continuity of displacement between the string at the coupling position and the other subsystem involved. Finally, the whole vibratory system is activated by an external force that represents the action of the finger on the key. The typical finger force profile is a step with given attack and release times.

### III. PHYSICAL MODELING USING THE U-K FORMULATION

#### A. U-K formulation for the clavichord

In this section, the clavichord model in terms of four coupled vibratory subsystems is modeled using a modal U-K formulation.<sup>20,21</sup> Let us consider a mechanical system

with mass matrix  $\mathbf{M}$ , which is subjected to a force vector  $\mathbf{F}_e(\mathbf{x}, \dot{\mathbf{x}}, t)$ , including all constraint-independent internal and external forces. This system is also subjected to constraining forces  $\mathbf{F}_c(t)$ . Denoting the dynamical solution  $\mathbf{y}_u(t)$  of the unconstrained system and  $\mathbf{y}(t)$  of the constrained system, the motion equations of the constrained system derived by Udwadia and Kalaba<sup>21,33</sup> are

$$\ddot{\mathbf{y}} = \ddot{\mathbf{y}}_u + \mathbf{M}^{-1/2} \mathbf{B}^+ (\mathbf{b} - \mathbf{A} \ddot{\mathbf{y}}_u), \quad \ddot{\mathbf{y}}_u = \mathbf{M}^{-1} \mathbf{F}_e(t), \quad (1)$$

where  $\mathbf{A}$  is the constraint matrix and  $\mathbf{b}$  the constrained vector obtained from  $P_h$  holonomic and  $P_{nh}$  non-holonomic constraints,  $\phi_p$  and  $\psi_p$ , respectively, defined as

$$\phi_p(\mathbf{y}, t) = 0, \quad p = 1, 2, \dots, P_h, \quad (2)$$

$$\psi_p(\mathbf{y}, \dot{\mathbf{y}}, t) = 0, \quad p = P_h + 1, P_h + 2, \dots, P_h + P_{nh}. \quad (3)$$

Time differentiation of Eqs. (2) and (3) gives the matrix-vector constraint equation in terms of accelerations,

$$\mathbf{A}(\mathbf{y}, \dot{\mathbf{y}}, t) \ddot{\mathbf{y}} = \mathbf{b}(\mathbf{y}, \dot{\mathbf{y}}, t). \quad (4)$$

Note that the generalized Moore–Penrose inverse matrix  $\mathbf{B}^+$  of  $\mathbf{B} = \mathbf{A} \mathbf{M}^{1/2}$  can be rendered numerically robust, even for a singular constraint matrix. For a particular external (finger) excitation  $\mathbf{F}_e(\mathbf{x}, \dot{\mathbf{x}}, t)$ , these equations are solved using a suitable time step integration scheme. A modal version of the U–K formulation suitable for continuous flexible systems like musical instruments is derived.<sup>21</sup> Assuming a set of  $S$  vibrating subsystems defined in terms of their unconstrained modal basis and coupled through  $P$  kinematic constraints, one obtains

$$\ddot{\mathbf{q}} = \mathbf{W} \tilde{\mathbf{M}}^{-1} (-\tilde{\mathbf{C}} \dot{\mathbf{q}} - \tilde{\mathbf{K}} \mathbf{q} + \mathbf{F}_{\text{ext}}), \quad (5)$$

where  $\mathbf{q}$  represents the vector of modal displacements;  $\tilde{\mathbf{M}}, \tilde{\mathbf{K}}, \tilde{\mathbf{C}}$  are, respectively, the modal mass matrix, modal stiffness matrix, and modal damping matrix; and  $\mathbf{W} = \mathbf{1} - \mathbf{M}^{-1/2} \mathbf{B} + \mathbf{A}$  is a global transformation matrix (which can conveniently be computed in advance of the time loop), where  $\mathbf{A}$  is the modal constraint matrix, and  $\mathbf{F}_{\text{ext}}$  are the external modal forces applied on the system.

#### B. Key-tangent modeling

A mode shape is associated with the key-tangent subsystem to model the tilting motion of the key. The modal representation of this system is given by

$$Y^k(x, t) = \phi^k(x) q^k(t), \quad (6)$$

where  $Y^k$  is the displacement of the key-tangent subsystem,  $\phi^k$  is its mode shape, and  $q^k$  is its modal amplitude, and

$$m^k \ddot{q}^k(t) + c^k \dot{q}^k(t) + k^k q^k(t) = F_{\text{ext}}(t), \quad (7)$$

where  $m^k$ ,  $c^k$ , and  $k^k$  are, respectively, the modal mass, modal damping, and modal stiffness of the key-tangent

subsystem, and  $F_{ext}$  is the modal excitation force that the musician exerts on the key. The key is modeled as a rigid body mode in rocking motion. The mode shape  $\phi^k$  is given in the following way:

$$\phi^k(x) = \frac{L_T - x}{L_T - L_p} - 1, \quad x \in [0, L_T]. \quad (8)$$

Let the linear density of the key be  $\rho_k = M_k/L_T$ . For any continuous linear system with density  $\rho$ , mode shape  $\phi_n$ , and length  $L$ , the modal mass  $m_n$  is

$$m_n = \int_0^L \rho \phi_n(x)^2 dx. \quad (9)$$

Then the modal mass of the key-tangent subsystem  $m^k$  is the sum of the tangent modal mass and that of the key,

$$m^k = M_{Tg} \phi^k(L_{tg})^2 + \int_0^{L_T} \rho_k \phi^k(x)^2 dx. \quad (10)$$

After some calculations, it gives

$$m^k = M_{Tg} \left( \frac{L_T - L_{tg}}{L_T - L_p} - 1 \right)^2 + M_k \frac{3L_p^2 - 3L_p L_T + L_T^2}{3(L_T - L_p)^2}. \quad (11)$$

### C. String modeling

#### 1. Modal description of the string

A modal representation of the string complying with the modal U–K formulation is given in this section. A modal expansion of the string displacement  $Y^S$  is

$$Y^S(x, t) = \sum_{n=1}^{N_s} \phi_n^S(x) q_n^S(t), \quad (12)$$

where  $\phi_n^S$  are the mode shapes of the string,  $q_n^S$  are its modal amplitudes, and  $N_s$  is the number of string modes. Considering that the boundary conditions of the clavichord string are pinned-pinned, one obtains the following string's mode shapes, for a string length  $L$ :

$$\phi_n^S(x) = \sin\left(\frac{n\pi x}{L}\right), \quad n = 1, 2, \dots, N. \quad (13)$$

For a large enough static displacement, the geometrical non-linear force  $F_{nl}^S$  related to the string's variation of tension needs to be considered. This yields the following string's modal equations:

$$M^S \ddot{\mathbf{q}}^S + C^S \dot{\mathbf{q}}^S + K^S \mathbf{q}^S + F_{nl}^S(\mathbf{q}^S, \dot{\mathbf{q}}^S) = \mathbf{0}, \quad (14)$$

where  $M^S$ ,  $C^S$ , and  $K^S$  are the modal mass matrix, the modal damping matrix, and the modal stiffness matrix of the string, respectively, and  $\mathbf{q}^S$  is the modal amplitude vector of the string. In Sec. III C 2, geometrical non-linear forces are expressed by means of the Kirchhoff–Carrier model.

### 2. Non-linear string dynamics in string-tangent interaction

The tangent lifts the string after the initial contact and increases the string tension. This displacement can be quite significant, up to 3–5 mm, inducing a substantial rise in pitch. The string uplift is a geometrical deformation, resulting in non-linear forces that must be considered in the dynamics of the instrument. For dynamic modeling of the non-linear forces, the Kirchhoff–Carrier non-linear string model is used,<sup>34,35</sup> following previous work on the 12-string Portuguese guitar.<sup>22,23</sup> Note that in this one-dimensional (1D) string motion model, all couplings between transverse and longitudinal motions are neglected. This seems to be a convenient approximation for 1D simulation; even if for small string vibratory amplitude, these couplings exist and are important for detailed potential energy considerations.<sup>36</sup>

According to the mode shapes in Eq. (13), the Kirchhoff–Carrier model leads to geometric non-linear terms for computing the dynamic tension  $T_{dyn}$ ,

$$T_{dyn}(t) = \frac{ES}{2L} \int_0^L \left[ \left( \frac{\partial Y^S(x, t)}{\partial x} \right)^2 \right] dx, \quad (15)$$

which gives rise to the non-linear differential equation of motion ( $T_0$  being the string tension at rest),

$$\rho S \frac{\partial^2 Y^S(x, t)}{\partial t^2} - (T_0 + T_{dyn}(t)) \frac{\partial^2 Y^S(x, t)}{\partial x^2} = 0. \quad (16)$$

The force  $F^{nl}$  due to geometric non-linear terms is

$$F^{nl}(x, t) = T_{dyn}(t) \frac{\partial^2 Y^S(x, t)}{\partial x^2}. \quad (17)$$

Thereby, it yields the non-linear modal force terms,

$$F_n^{nl}(t) = \int_0^L F^{nl}(x, t) \phi_n(x) dx. \quad (18)$$

Using Eqs. (12) and (13) and calculating the integrals in Eq. (15) gives the dynamic tension that depends quadratically on the modal response amplitudes,

$$T_{dyn}(t) = \frac{ES\pi^2}{4L^2} \sum_{n=1}^N n^2 (q_n(t))^2. \quad (19)$$

Then, calculating the integral in Eq. (18), the cubic modal force terms are deduced,<sup>22</sup>

$$F_n^{nl} = \frac{ES\pi^4}{8L^3} n^2 q_n(t) \sum_{m=1}^N m^2 q_m(t)^2. \quad (20)$$

Equation (20) represents the modal non-linear forces for the string due to the vertical displacement resulting from the tangent lift. In contrast to the quasi-static situation, the force in Eq. (20) can be computed in dynamic modeling of this interaction. The increase in tension due to tangent height  $Y_e$  is an

important parameter for the player, as it is related to the hardness of touch,<sup>5</sup> i.e., the key force feedback felt by the player.

### 3. Model of string's modal dampings

The string model by Valette and Cuesta<sup>37</sup> is chosen to bestow a proper damping coefficient to each string mode. The air friction, the visco-elastic and thermo-elastic friction, and the structural friction are taken into account and represented by the quality factors  $Q_{n,air}$ ,  $Q_{n,ve-te}$ , and  $Q_{struc}$ , respectively,

$$Q_n^{-1} = Q_{n,air}^{-1} + Q_{n,ve-te}^{-1} + Q_{struc}^{-1} = \frac{R}{2\pi\rho_L} (nf_0)^{-1} + \frac{4\pi^2\rho_L EI\delta_{ve}}{T^2} (nf_0)^2 + Q_{struc}^{-1}, \quad (21)$$

where  $R$  stands for mechanical resistance,

$$R = 2\pi\eta + 2\pi d_s \sqrt{\pi\eta_{air}\rho_{air}f}, \quad (22)$$

and where  $\rho_{air}$  and  $\eta_{air}$  correspond to the dynamic viscosity and the density of the air, respectively, and  $d_s$  represents the string's diameter. Then  $Q_n^{-1}$  represents the damping coefficient associated with the  $n$ th mode of the string,  $E$  is the Young's modulus of the string,  $I$  is the second moment of inertia of the string,  $T$  is the string's tension,  $\rho_L$  is the linear density of the string, and  $\delta_{ve-te}$  is the imaginary part of the string Young's modulus. The term  $\delta_{ve-te} = \delta_{ve} + \delta_{te}$  encapsulates visco-elastic effects  $\delta_{ve}$  and thermo-elastic ones  $\delta_{te}$ , taking the same approach as Ref. 29.  $Q_{struc}$  is a constant value. Using  $\zeta_n = Q_n^{-1}/2$ , one can obtain the damping  $\zeta_n$  coefficients of the string.

### D. Bridge modeling

The motion of the bridge is modeled using modal equations. Modal expansion of the bridge displacement is

$$Y^B(s, t) = \sum_{n=1}^{N_B} \phi_n^B(s) q_n^B(t), \quad (23)$$

where  $s$  is the curvilinear coordinate position on the bridge,  $N_B$  is the number of bridge modes,  $\phi_n^B$  are the mode shapes of the bridge, and  $q_n^B$  are the modal amplitudes of the bridge. Modal equations governing the bridge's vibratory motion are

$$M^B \ddot{\mathbf{q}}^B + C^B \dot{\mathbf{q}}^B + K^B \mathbf{q}^B = \mathbf{0}, \quad (24)$$

where  $M^B$ ,  $C^B$ , and  $K^B$  are the modal mass matrix, the modal damping matrix, and the modal stiffness matrix of the bridge, respectively, and  $\mathbf{q}^B$  is the modal amplitude vector of the bridge. Because of the complexity of the structure, as opposed to the string, analytical expression cannot be derived for bridge modal equations. Numerical values to the

bridge modal parameters are obtained by experimental modal analysis (Sec. II E).

### E. Damper modeling

The damper is modeled by coupling a portion of string with a number of mass-spring-dampers, assuming a continuity of displacement between the dampers and the string at their contact points. All these mass-spring-dampers are considered independent of one another. The modal equations governing the dampers' vibratory motion are

$$M^D \ddot{\mathbf{q}}^D + C^D \dot{\mathbf{q}}^D + K^D \mathbf{q}^D = \mathbf{0}, \quad (25)$$

where  $\mathbf{q}^D$  is the amplitude vector of the damper responses. The length of  $\mathbf{q}^D$  is  $N_D$ , the number of dampers. Matrices  $M^D$ ,  $C^D$ , and  $K^D$  are square diagonal with identical coefficients  $m^D$ ,  $c^D$ , and  $k^D$ , respectively. All the mass-spring-dampers associated with the cloth damping device have the same mass, stiffness, and damping coefficients. Thus, all the mass-spring-dampers have the same frequency and the same damping. These mass-spring-dampers representing the cloth damper are coupled with a certain length of the string, as described in Sec. III F 3.

### F. Couplings between subsystems

The individual subsystems are described with the help of a modal representation. The modal constraint matrix  $A$  and the vector  $\mathbf{b}$  of the constrained system are given by  $A\ddot{\mathbf{Q}} = \mathbf{b}$ , with

$$A = \begin{bmatrix} A^B \\ A^k \\ A^D \end{bmatrix}, \quad \mathbf{b} = \begin{bmatrix} \mathbf{b}^B \\ b^k \\ \mathbf{b}^D \end{bmatrix}, \quad \ddot{\mathbf{Q}} = \begin{bmatrix} \ddot{\mathbf{q}}^S \\ \ddot{\mathbf{q}}^B \\ \ddot{q}^k \\ \ddot{\mathbf{q}}^D \end{bmatrix}, \quad (26)$$

where  $A^B$  is the matrix coupling the string with the bridge with  $\mathbf{b}^B$  its associated vector,  $A^k$  is the matrix coupling the string with the key-tangent subsystem with  $b^k$  its associated vector, and  $A^D$  is the matrix coupling the string with the damper with  $\mathbf{b}^D$  its associated vector. Given the continuity conditions for coupling, these matrices and vectors are derived in Secs. III F 2, III F 1, and III F 3.

#### 1. String and key-tangent subsystem coupling

When the tangent touches the string, coupling between the two subsystems occurs. At the contact location, assuming a continuity of displacement between the two subsystems, the coupling conditions are

$$Y^S(x_{ext}, t) - Y^k(L_{tg}, t) = 0, \quad (27)$$

$$[\Phi^S(x_{ext})]^T \mathbf{q}^S(t) - \Phi^k(L_{tg}) q^k(t) = 0, \quad (28)$$

where  $Y^k$  is the displacement of the tangent, and  $x_{ext}$  is the position where the string is excited. The tangent is initially located below the string with respect to axis  $y$ . The whole string is initially at rest at altitude  $y=0$ . At the moment when the tangent reaches altitude  $y=0$ ,  $A^k$  must be modified to couple the two subsystems. The coupling conditions are

$$\left\{ \begin{array}{l} \text{If } Y^k(L_{tg}, t) < Y^S(x_{ext}, t) \\ \Rightarrow b^k = 0 \\ \text{and } A^k = \mathbf{0} \\ \\ \text{If } Y^k(L_{tg}, t) = Y^S(x_{ext}, t) \\ \Rightarrow b^k = 0 \\ \text{and } A^k = \left[ [\Phi^S(x_{ext})]^T \ 0 \dots 0 \ -\Phi^k(L_{tg})^T \ 0 \dots 0 \right]. \end{array} \right.$$

The U–K formulation applies constraints on the system acceleration. Respecting the constraints on acceleration does not imply respecting the constraints on the system displacement and velocity. Stabilization techniques are needed to avoid numerical drifts during the simulation because of the displacement and velocity constraint violation. The technique used here is based on a geometric projection approach, applied after each time step  $t_k$ , when small computational errors lead to violations of the holonomic  $\varphi(\mathbf{q}(t_k)) \neq \mathbf{0}$  and non-holonomic constraints  $\Psi(\mathbf{q}(t_k), \dot{\mathbf{q}}(t_k)) \neq \mathbf{0}$ , expressed in terms of their modal coordinates and velocities. Following Yoon *et al.*,<sup>38</sup> the displacement constraint violations are cancelled by perturbing the solution  $\mathbf{q}(t_k)$ , so that the corrected solution  $\mathbf{q}_c(t_k) = \mathbf{q}(t_k) + \delta\mathbf{q}(t_k)$  perfectly copes with the constraints  $\varphi(\mathbf{q}_c(t_k)) = \mathbf{0}$ . This yields<sup>39</sup>

$$\begin{aligned} \varphi(\mathbf{q}_c(t_k)) &= \mathbf{0} \\ \Rightarrow \varphi(\mathbf{q}(t_k) + \delta\mathbf{q}(t_k)) &= \mathbf{0} \\ \Rightarrow \varphi(\mathbf{q}(t_k)) + \delta\varphi &= \mathbf{0}, \end{aligned} \tag{29}$$

with the constraint perturbation given by

$$\delta\varphi = \sum_{n=1}^N \frac{\partial\varphi}{\partial q_n} \delta q_n = \mathbf{A}\delta\mathbf{q}, \tag{30}$$

where  $\mathbf{A}$  denotes the constraint gradient matrix, in terms of the modal coordinates, which is typically non-square. Then from Eqs. (29) and (30) stems the following constraint-enforcing correction:

$$\begin{aligned} \varphi(\mathbf{q}(t_k)) + \mathbf{A}\delta\mathbf{q} &= \mathbf{0} \\ \Rightarrow \delta\mathbf{q} &= -\mathbf{A}^+\varphi(\mathbf{q}(t_k)) \\ \Rightarrow \mathbf{q}_c(t_k) &= \mathbf{q}(t_k) - \mathbf{A}^+\varphi(\mathbf{q}(t_k)), \end{aligned} \tag{31}$$

where  $\mathbf{A}^+$  is the Moore–Penrose pseudo-inverse of matrix  $\mathbf{A}$ . When non-holonomic constraints are applied, a procedure similar to Eq. (31) may be used for the corrected

velocities  $\dot{\mathbf{q}}_c(t_k) = \dot{\mathbf{q}}(t_k) + \delta\dot{\mathbf{q}}(t_k)$ , which perfectly cope with the velocity constraints  $\Psi(\mathbf{q}_c(t_k), \dot{\mathbf{q}}_c(t_k)) = \mathbf{0}$ . Then

$$\begin{aligned} \Psi(\mathbf{q}_c(t_k), \dot{\mathbf{q}}_c(t_k)) &= \mathbf{0} \\ \Rightarrow \Psi(\mathbf{q}_c(t_k), \dot{\mathbf{q}}(t_k) + \delta\dot{\mathbf{q}}(t_k)) &= \mathbf{0} \\ \Rightarrow \Psi(\mathbf{q}_c(t_k), \dot{\mathbf{q}}(t_k)) + \delta\Psi &= \mathbf{0}, \end{aligned} \tag{32}$$

with the constraint perturbation given by

$$\delta\Psi = \mathbf{A}\delta\dot{\mathbf{q}}, \tag{33}$$

and from Eqs. (32) and (33) stems the following constraint-enforcing correction:

$$\begin{aligned} \Psi(\mathbf{q}_c(t_k), \dot{\mathbf{q}}(t_k)) + \mathbf{A}\delta\dot{\mathbf{q}} &= \mathbf{0} \\ \Rightarrow \delta\dot{\mathbf{q}} &= -\mathbf{A}^+\Psi(\mathbf{q}_c(t_k), \dot{\mathbf{q}}(t_k)) \\ \Rightarrow \dot{\mathbf{q}}_c(t_k) &= \dot{\mathbf{q}}(t_k) - \mathbf{A}^+\Psi(\mathbf{q}_c(t_k), \dot{\mathbf{q}}(t_k)). \end{aligned} \tag{34}$$

## 2. String-bridge coupling

The string and bridge are coupled, assuming a continuity of the string and bridge displacements at the string-bridge contact point: the string displacement  $Y^S(x_B, t)$  must be the same as that of the bridge  $Y^B(x_B, t)$ , where  $x_B$  is the location of the coupling point on the string and  $x_B$  is the location of the coupling point on the bridge,

$$Y^S(x_B, t) - Y^B(x_B, t) = 0. \tag{35}$$

With modal coordinates, it leads to

$$[\Phi^S(x_B)]^T \mathbf{q}^S(t) - [\Phi^B(x_B)]^T \mathbf{q}^B(t) = 0, \tag{36}$$

with the mode shape vectors

$$\begin{aligned} \Phi^S(x_B) &= [\phi_1^S(x_B)\phi_2^S(x_B)\dots\phi_{N_S}^S(x_B)]^T, \\ \Phi^B(x_B) &= [\phi_1^B(x_B)\phi_2^B(x_B)\dots\phi_{N_B}^B(x_B)]^T, \end{aligned} \tag{37}$$

where  $N_B$  is the number of bridge modes, and  $N_S$  is the number of string modes. Equation (38) shows the string-bridge coupling matrix  $\mathbf{A}^B$  and the associated vector  $\mathbf{b}^B$ ,

$$\mathbf{A}^B = \left[ [\Phi^S(x_B)]^T \quad -[\Phi^B(x_B)]^T \quad 0 \quad \dots \quad 0 \right]. \tag{38}$$

## 3. String-damper coupling

For string-damper coupling, continuity of the string's displacement  $Y^S(x_D, t)$  with that of the damper  $Y^D(\mathbf{r}_s, t)$  is assumed,  $x_D$  being the location of the damper on the string,

$$Y^S(x_D, t) - Y^D(x_D, t) = 0, \tag{39}$$

$$[\Phi^S(x_D)]^T \mathbf{q}^S(t) - \mathbf{q}^D(t) = 0. \tag{40}$$

Equation (40) leads to the following matrix  $A^D$  and vector  $\mathbf{b}^D = \mathbf{0}$ , where  $\Phi^S(x_{D_i})$  is the mode shape of the string coupled with the  $n$ th damper at the  $x_{D_i}$  location:

$$A^D = \begin{bmatrix} [\Phi^S(x_{D_1})]^T & 0 & \cdots & 0 & -1 & 0 & \cdots & 0 \\ [\Phi^S(x_{D_2})]^T & 0 & \cdots & 0 & 0 & -1 & \cdots & 0 \\ \vdots & \vdots & \ddots & \vdots & \vdots & \vdots & \ddots & \vdots \\ [\Phi^S(x_{D_{N_D}})]^T & 0 & \cdots & 0 & 0 & 0 & \vdots & -1 \end{bmatrix}$$

#### IV. SIMULATION AND EVALUATION OF THE CLAVICHORD MODEL

In this section, assessment of the model is performed along three lines—string motion, tangent-string interaction, and bridge vibration—by comparing simulated and experimental data. A finite difference approach is chosen for simulation of the one-string model developed in Sec. III, using the experimental data of Sec. II. The time step for simulation is chosen according to an energy analysis of the simulation (using  $N_s = 150$  string modes). This energy analysis studies the work done by the key-tangent subsystem compared to total energy of the coupled system for different time steps. The energy provided to the system is the work  $E_e = \sum_{n=1}^N E_{e,n}$  done by the tangent, with the modal work  $E_{e,n}$ ,

$$E_{e,n}(t) = \int_0^t F_{ext,n}(t) \dot{q}_n^k(t) dt. \quad (41)$$

The sum of all modes' energy of the string, of the system tangent-key, of the damper, and of the bridge gives the total energy of the modeled system. Results reported in Fig. 5 show that the total energy converges toward the key-tangent subsystem work as the time step decreases.

Given the energy analysis of the simulated model, a time step of  $\Delta t = 2 \times 10^{-6}$  s has been chosen to ensure a realistic simulation. A smaller time step gives a better fit

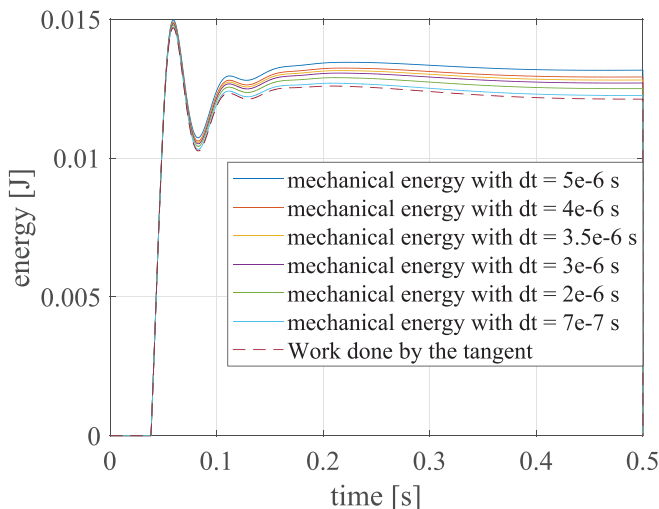


FIG. 5. (Color online) Convergence of the total mechanical energy of the system compared to the work done by the tangent.

between the work done by the key-tangent subsystem and the total energy of the coupled system, but it does not greatly improve the auditory or visual quality of the simulation when it greatly increases the computational load.

Assessment of the model is performed in three steps: (1) visualization of string motion; (2) tangent-string interaction and dynamics of the clavichord; and (3) bridge vibrations and comparison with experimental data.

#### A. String motion

The string motion of the clavichord is shaped by the specific excitation mechanism of the instrument. Simulation of the G#<sub>3</sub> string motion is displayed in Fig. 6, in response to a 4.2 N excitation force applied on the key. The same data are better visualized in the associated video Mm. 3, displaying evolution of the string and tangent motions in time. Figure 6(a) represents the initial 4 ms, i.e., the beginning of the motion. The tangent (represented by circles at  $x = 0.6$  m, sampled with a period of 0.05 ms) comes in contact with the string and lifts the string to a maximum. When the tangent strikes the string, an angular point is created and propagates to the bridge. At the same time, the string is uplifted by the tangent. After the arrival of the angular point at the bridge, it is reflected back and then reflected again by the tangent. As the mechanical impedance of the bridge and that of the tangent are high compared to the string mechanical impedance, most of the wave energy is reflected. Vibratory amplitude (then the sound amplitude level) depends on the angle of the angular point and then on the ratio of wave velocity in the string and tangent velocity, as discussed in Ref. 8, and then on the steepness of the tangent motion slope. In Fig. 6(b), the string motion history is displayed between 7 and 57 ms (sampled with a period of 0.5 ms). The low frequency (81 Hz) oscillation of the key-tangent subsystem because of the elasticity of the string is observed. Figure 6(c) shows vibration of the sympathetic part of the string between the bridge and tuning pin, between 9 and 17 ms (sampled with a period of 0.05 ms). Note that this vibration is 2 orders of magnitude lower than the played part of the string, between  $10^{-5}$  and  $10^{-6}$  m, and that the string motion looks rather disorganized compared to the more regular motion between the tangent and bridge pin. This figure and associated video (Mm. 3) represent the first visualization of simulated clavichord string motion to the best of our knowledge. Comparison with high-speed videos of the string motion in the vicinity of the tangent<sup>40</sup> shows good agreement with the simulation.

Mm. 3. Video of the simulated clavichord string displacement and velocity at the top and at the bottom respectively. This is a file of type “mov” (17.76 MB).

#### B. Tangent-string dynamics

Tangent-string dynamics is an essential feature of the clavichord dynamics, tangent velocity and displacement

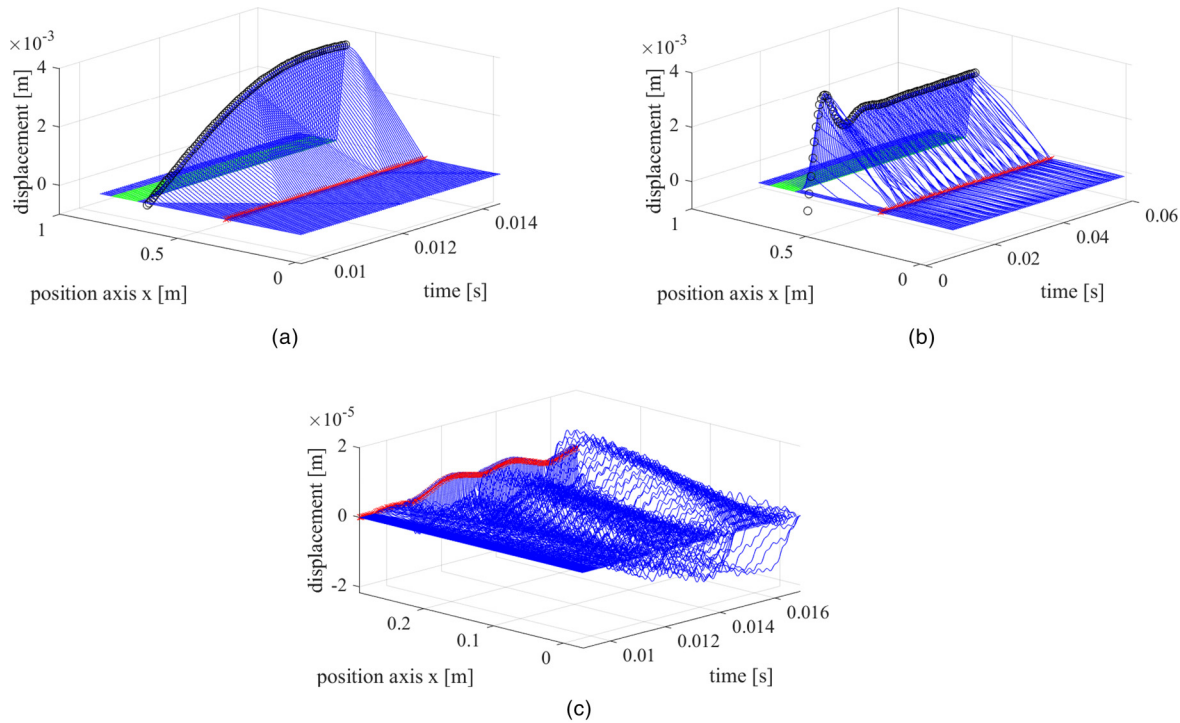


FIG. 6. (Color online) History of the transverse motion for the G#<sub>3</sub> string. *x* axis: time; *y* axis: string length; *z* axis: transverse string motion. (a) Full string between  $t = 10.0$  ms and  $t = 14.0$  ms; (b) full string between  $t = 7.0$  ms and  $t = 57.0$  ms; (c) sympathetic part alone, between  $t = 9.0$  ms and  $t = 17.0$  ms.

being the main control parameters for the performer. Figure 7 shows the velocity of the contact point between the tangent and the key. As expected,<sup>8</sup> the key-tangent system oscillates, because of the string elastic reaction to the tangent uplift. The simulated oscillation frequency is 81 Hz [peak velocity  $1.279 \text{ m s}^{-1}$ , Fig. 7(a)], compared to the 40 Hz measured oscillation frequency [peak velocity  $1.135 \text{ m s}^{-1}$ , Fig. 7(b)]. The vertical tangent velocity is measured using a Brüel & Kjær (Nærum, Denmark) 4374 miniature high-sensitivity accelerometer attached to the key, close to the tangent, and a conditioning amplifier, Brüel & Kjær 2635. With an accelerometer mass of  $\approx 0.75 \text{ g}$  and a key mass of  $\approx 20 \text{ g}$ , the mass weighting effect of the accelerometer is neglected. This frequency difference could be explained by the lack of finger weight in the model. Finger weight would provide additional mass to the key-tangent subsystem, decreasing its oscillation frequency. In this “light key” simulation, the key-tangent subsystem modal mass is  $1.17 \times 10^{-2} \text{ kg}$ , with a damping coefficient of  $2.5 \text{ kg s}^{-1}$ . A “heavy key” simulation [Fig. 7(c)], where the key-tangent subsystem modal mass becomes  $2.87 \times 10^{-2} \text{ kg}$  and its damping coefficient is  $3.5 \text{ kg s}^{-1}$ , is consistent with measurements. Because the key is heavier in this case, the tangent impact velocity decreased (peak velocity  $0.928 \text{ m s}^{-1}$ ).

Figure 8 shows the effect of the tangent uplift on string tension. Simulated tangent uplift changes the measured<sup>41</sup> fundamental frequency. This is consistent with measured data and quasi-static modeling results published earlier.<sup>8</sup> The tangent displacement controls pitch.

To study the effect of tangent velocity on acceleration at the bridge, the force  $F_{ext}$  applied on the key-tangent

subsystem is varied. The impact velocity and the average acceleration are computed by the model. Similarly to the SPL, the acceleration level is computed as the logarithm of acceleration integrated over 250 ms. Figure 9 shows a linear relationship between the logarithm of the impact velocity and the acceleration level in dB. This is in good agreement with experimental results obtained for impact velocity and SPL and with predictions by a linear model of string-tangent dynamics.<sup>8</sup> Playing faster results in playing louder.

The influence of the impact velocity on the timbre of the bridge acceleration is studied. Spectral slopes of the acceleration spectrum for different impact velocities of the key-tangent subsystem ( $0.4433, 0.535, 0.622, 0.698, 0.769, 0.834, 0.894,$  and  $0.951 \text{ m s}^{-1}$ ) are presented in Fig. 10. Two effects are noticeable. First, increasing the excitation force leads to increasing the static displacement of the string, hence the fundamental frequency. This accounts for the frequency shift of the partials in Fig. 10. Second, the spectral slopes for the different spectra remain on average identical. This spectral slope of the simulated bridge acceleration is consistent with the SPL spectral slope variation with respect to the tangent impact velocity reported earlier.<sup>8</sup> Playing louder does not greatly change the clavichord’s timbre.

### C. Bridge vibration

Bridge vibration assessment is essential, because bridge vibration results in soundboard vibration and then sound radiation. For assessment of the model, simulated and measured bridge motions are compared. A robotic finger<sup>42</sup> is used for measurement. The robotic finger presses the key

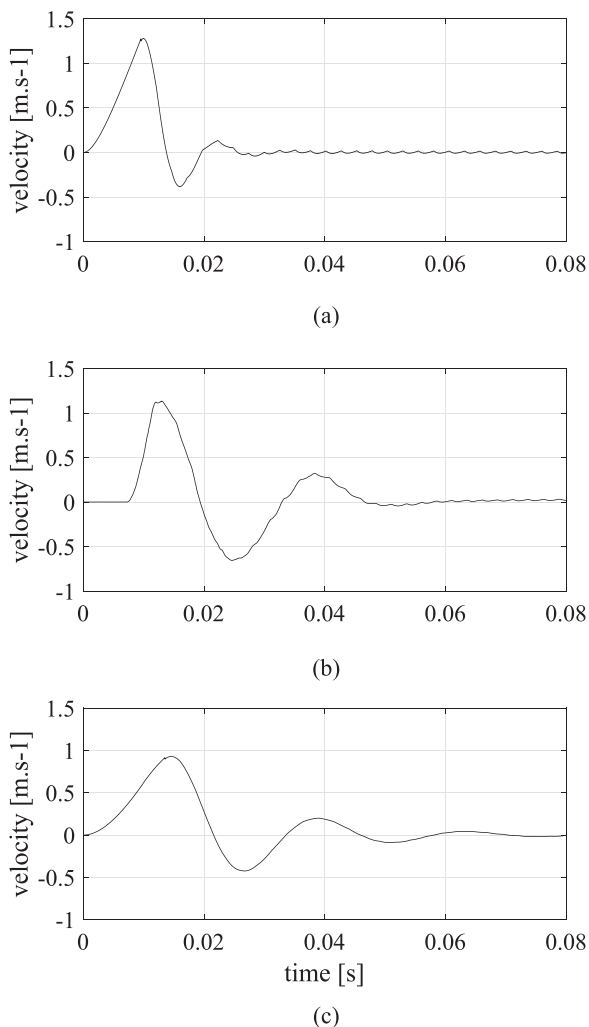


FIG. 7. Comparison of simulated and measured velocity at the tangent-string contact point. (a) "Light key" simulation; (b) measurement; (c) "heavy key" simulation.

following a programmed vertical motion for the string under study. All other strings are muffled using felt strips.

Measurement of acceleration at the bridge pin follows the procedure described in Sec. II E. The first simulation takes into account all the bridge modes identified in Sec. II E up to 3500 Hz. The second simulation takes into account the first 31 identified bridge modes, leading to a modal truncation of the bridge at 600 Hz. Measured and

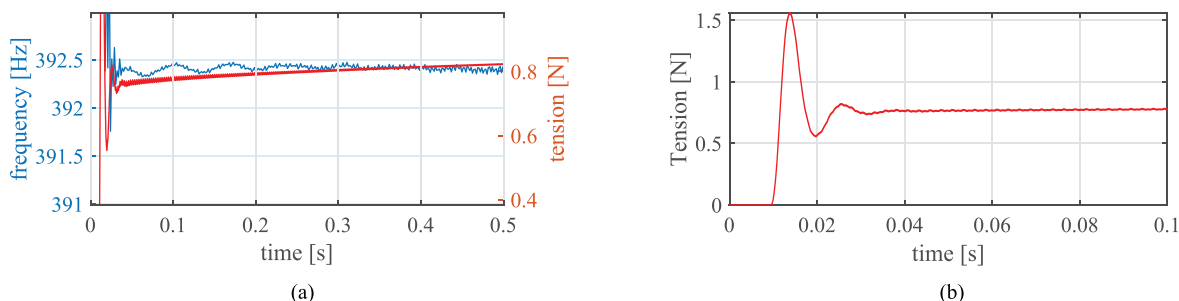


FIG. 8. (Color online) (a) Dynamic tension of the string (red) and corresponding fundamental frequency (blue) for a 0.5 s note; (b) zoom of this same dynamic tension of the string in the first 0.1 s.

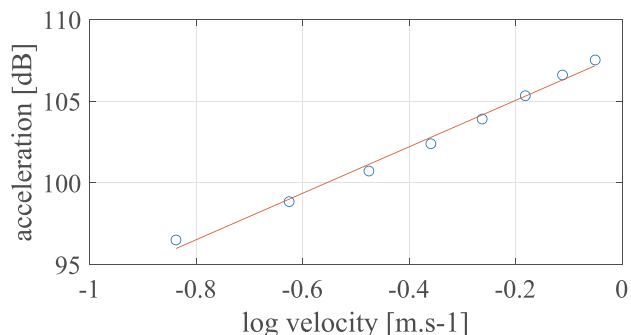


FIG. 9. (Color online) Logarithmic bridge acceleration (ref 1 dB: 1 m s<sup>-2</sup>) as a function of the logarithmic tangent impact velocity.

simulated signal waveforms are displayed in Fig. 11, together with corresponding sound example Mm. 4 (measured signal), sound example Mm. 5 (modal truncation at 3500 Hz), and sound example Mm. 6 (modal truncation at 600 Hz). Figure 12 gives a closer look at details of the three waveforms in Fig. 11 at 0.01, 0.1, and 0.31 s, respectively. The visual and sound results show good general agreement between measurement and simulation. The effect of modal truncation on the high frequency content of the simulated waveforms is clearly observed. The main difference between measurement and simulation is observed in the attack transient. This could be explained by the structural noise noticeable in a real clavichord but not taken into account in the model. Structural noise results from the shock of the tangent on the string, which excites all the case of the instrument, and coupling of the whole the string band through the damper (often coined as "drum noise").

- Mm. 4. Sound of the measured acceleration at the G#<sub>3</sub> string/bridge coupling point. This is a file of type "wav" (101 KB).
- Mm. 5. Sound of the simulated acceleration at the G#<sub>3</sub> string/bridge coupling point with a modal truncation at 3500 Hz. This is a file of type "wav" (196 KB).
- Mm. 6. Sound of the simulated acceleration at the G#<sub>3</sub> string/bridge coupling point with a modal truncation at 600 Hz. This is a file of type "wav" (196 KB).

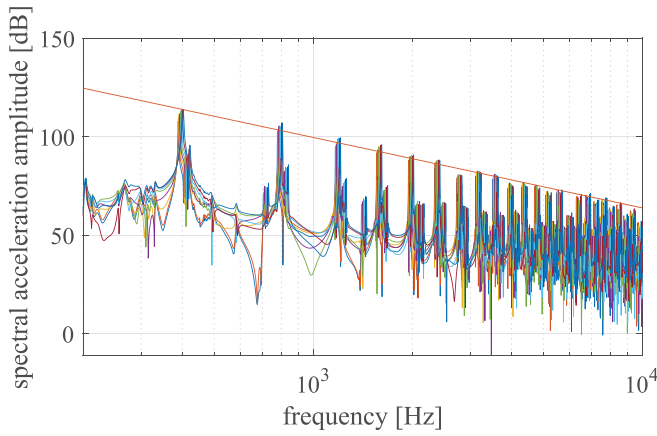


FIG. 10. (Color online) Logarithmic spectral magnitude of bridge acceleration (ref 1 dB:  $1 \text{ m s}^{-2}$ ) for different impact velocity of the key-tangent sub-system with the average spectral slope.

Finally, the forces applied to the key and the response at the bridge are analyzed with the help of Fig. 13. A step force of 4.2 N is applied on the key for 1 s. The constraint force at the contact point between the tangent and strings is computed. Note that the tangent force is lower than the force applied to the key because of the leverage ratio of the pivoting key (since  $x_f - x_p$  is smaller than  $x_p - x_{tg}$ ); see Fig. 13(c). Two conditions are studied in the simulation

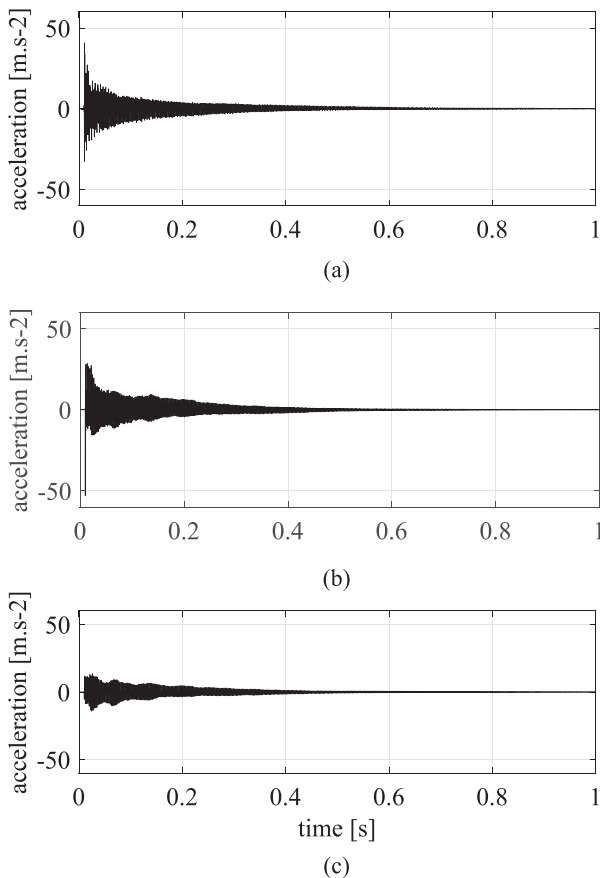


FIG. 11. Bridge acceleration waveforms (1 s). (a) Measurement; (b) simulation (3500 Hz modal truncation); (c) simulation (600 Hz modal truncation).

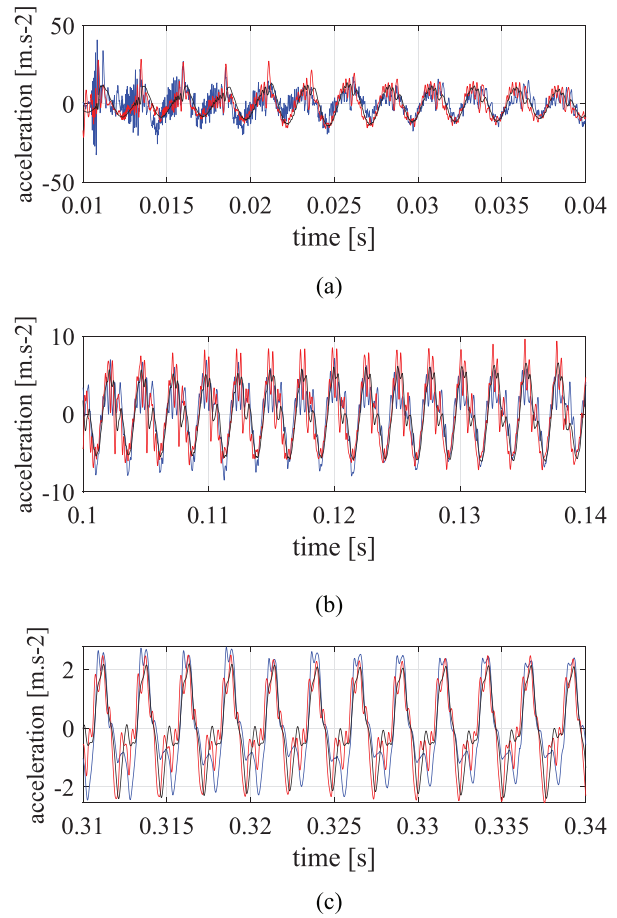


FIG. 12. (Color online) Bridge acceleration waveforms at different times: measurement in blue, simulation (3500 Hz modal truncation) in red, and simulation (600 Hz modal truncation) in black; (a) from  $t=0.01 \text{ s}$  to  $t=0.04 \text{ s}$ ; (b) from  $t=0.1 \text{ s}$  to  $t=0.14 \text{ s}$ ; (c) from  $t=0.31 \text{ s}$  to  $t=0.34 \text{ s}$ .

with and without the damper subsystem. Figure 13(b) shows the simulated force at the bridge. As expected, the force is lowered during the tone because the tangent lifts the string and then releases the string pressure on the bridge. When the damper subsystem is removed, the string appears less constrained, and the force lowering is higher. String vibration is apparent in the force signal. Figure 13(a) shows the vibration displacement. As expected, the string is raised in response to the tangent lift and raised higher when the dampers are withdrawn. The vibratory magnitude is surprisingly low (a maximum of about 0.015 mm). For assessment, displacement measurements are performed on the  $G\#_3$  string using a Keyence (LJ-V7060) profilometer. The same order of magnitude is observed: a bridge lift of 0.010–0.020 mm and a maximal vibratory amplitude of about 0.010–0.015 mm, a result that is in good agreement with the simulation. After the key release, the tangent loses contact with the string. The remaining vibration after the key release corresponds to the sympathetic vibration between the bridge and tuning pin and, in the non-damped situation, to the vibration of all the length of the string. In this latter situation, the magnitude is larger.

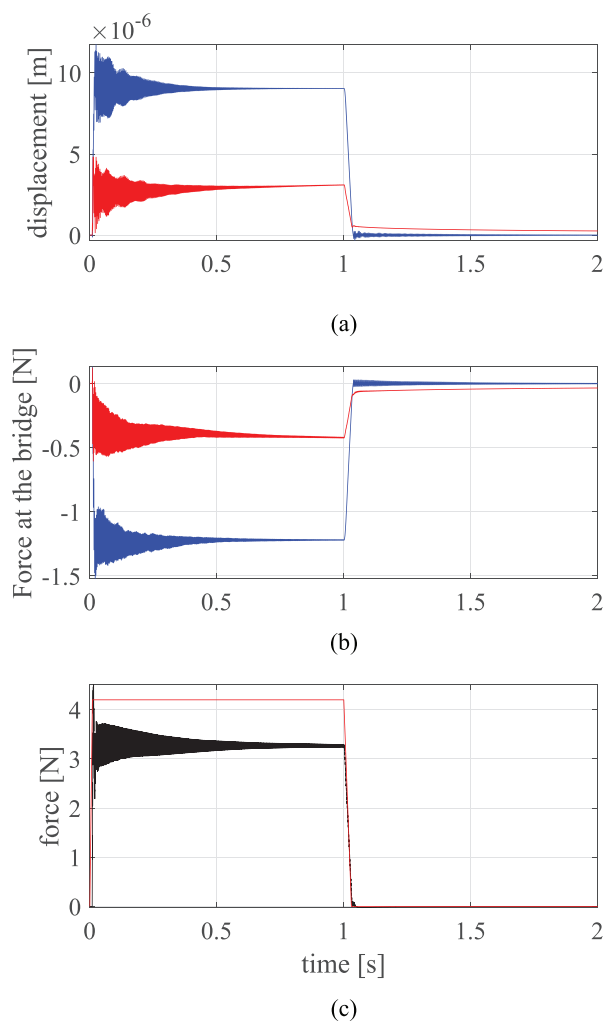


FIG. 13. (Color online) (a) Bridge displacement with (red) and without (blue) dampers; (b) force on the bridge with (red) and without (blue) dampers; (c) force applied on the key and resulting force on the tangent.

## V. CONCLUSION AND PERSPECTIVES

Time-domain physical simulation of a simplified clavichord model is developed in this paper, together with measurements on a functional instrument. The clavichord is considered as a constraint system made of four vibratory coupled subsystems: key-tangent, string, damper, and bridge-soundboard. In the first part, modal, dynamic, and motion parameters for the four subsystems are measured on the clavichord under study. Various measurement techniques and devices are used: experimental modal analysis for the bridge, soundboard, and key (accelerometers and impact hammer); string damping characteristics (isolated string bench and optical forks); tangent and string motions (accelerometer and laser vibrometer); and applied force on the key (robotic finger). These experimental results are useful for simulation assessment in this paper as well as for reference for future studies of other instruments. The second part is devoted to simulation. The U-K formulation is chosen because of its compatibility with a modal representation for coupled vibratory subsystems. Modal representations for the

string, bridge, key-tangent, and damper subsystems are developed. Another key point in this work is dynamic modeling of geometrical non-linear forces resulting from the string uplift by the tangent, with the help of the Kirchoff-Carrier model. Conditions of continuity in displacement between each subsystem are considered to derive the coupling matrix of the constraint system. String excitation is obtained by coupling the key-tangent subsystem and the string at the moment of contact. The constraint force uplifts the string and sets the string into vibration. Coupling between the string and the key-tangent subsystem requires a stabilization technique to correct constraint violation for the displacement and the velocity because two subsystems are not exactly in the same position at the contact moment. In the third part, simulation results are compared with experimental results. A suitable time step for time-domain simulation is chosen according to an energy convergence analysis. The key-tangent and string dynamic of the model is compared to measurements. Low frequency oscillation and dynamic tension variation of this subsystem are successfully rendered by the model. This is on the side of the performer's fingers. Simulated string motion is realistic, and the associated video showing velocity and displacement of the simplified model is in our opinion the highlight of the present paper. Bridge motion can be considered as the source of the radiated sound. Realistic force, displacement, and acceleration waveforms (with associated sound examples) are obtained in response to the force applied on the key. This is on the side of the performer's ears. Results on the dynamics of the clavichord reported earlier in the literature are found in the simulation: linear relationship between the bridge log acceleration and log peak tangent velocity, pitch variation as a function of key uplift height, and bridge acceleration with almost constant spectral slope for different tangent impact velocities.

A simplified one-string instrument is simulated here. Important vibro-acoustic characteristics of the clavichord are therefore missing and must be worked out. For most instruments, the tangent strikes a choir of unison strings. This influences considerably the clavichord sound, as the two unison strings are not struck exactly at the same time by the tangent. The sound of the clavichord is influenced by the vibration of the sympathetic strings, creating a reverberation effect and sometimes "wolf" notes. Sound radiation by the soundboard, reflection by the lid, and structural noise must be studied. Needless to say, a full model of the instrument should include all the strings. We believe the approach presented here forms a solid basis for such a project, aiming at a fully parametric physical clavichord model that would be desirable for historical instrument simulation and analysis, performance studies, and new music instrument design.

## ACKNOWLEDGMENTS

The authors wish to thank the two anonymous reviewers and Thomas Steiner (Basel) for their criticisms

and suggestions that helped much in clarifying and improving both the content and form of this work.

- <sup>1</sup>G. Crowell, "Every player's first grammatica," De Clavicordio VI, Proceedings of the International Clavichord Symposium, Magnano, Italy (September 10–13, 2003), edited by B. Brauchli, A. Galazzo, and I. Moody, pp. 53–60.
- <sup>2</sup>B. Brauchli, *The Clavichord* (Cambridge University, Cambridge, UK, 1998).
- <sup>3</sup>F. Trendelenburg, E. Franz, and E. Thienhaus, *Zur Klangwirkung von Klavichord, Cembalo und Flügel (On the Sound Effect of the Clavichord, Harpsichord and Grand Piano)* (Siemensstadt, Berlin, 1940).
- <sup>4</sup>R. A. Hands, "A scientific approach to the clavichord," *Galpin Soc. J.* **20**, 89–98 (1967).
- <sup>5</sup>P. Bavington, "Keylever, tangent and string—A preliminary analysis of clavichord touch and action," De Clavicordio III, Proceedings of the International Clavichord Symposium, Magnano, Italy (September 24–28, 1997), edited by Be. Brauchli, S. Brauchli, and A. Galazzo.
- <sup>6</sup>S. Thwaites and N. H. Fletcher, "Some notes on the clavichord," *J. Acoust. Soc. Am.* **69**(5), 1476–1483 (1981).
- <sup>7</sup>D. E. Hall, "String excitation: Piano, harpsichord and clavichord," in *Proceedings of the 1993 Stockholm Music Acoustics Conference*, Stockholm (July 28–August 1, 1993), pp. 309–314.
- <sup>8</sup>C. d'Alessandro, "On the dynamics of the clavichord: From tangent motion to sound," *J. Acoust. Soc. Am.* **128**(4), 2173–2181 (2010).
- <sup>9</sup>C. d'Alessandro, C. Besnainou, and L. Giniéis, "Tonal portrait of the clavichord," De Clavicordio VIII, Proceedings of the International Clavichord Symposium, Magnano, Italy (September 5–8, 2007), edited by B. Brauchli, A. Galazzo, J. Wardman, pp. 201–213.
- <sup>10</sup>C. d'Alessandro, "Le paradoxe du clavicorde et la technique de bach au clavier" ("The clavichord paradox and Bach's keyboard technique"), *Rev. Music. OICRM* **6**(1), 87–112 (2019).
- <sup>11</sup>V. Välimäki and C. Erkut, "Commutated waveguide synthesis of the clavichord," *Comput. Music J.* **27**(1), 71–82 (2003).
- <sup>12</sup>See <https://modartt.com/neupert> for listening the physical model of a clavichord (Last viewed 9/20/21).
- <sup>13</sup>J. Chabassier, "Modélisation et simulation numérique d'un piano par modèles physiques" ("Modeling and numerical simulation of a piano"), Ph.D. thesis, Ecole Polytechnique X, Palaiseau, France, 2012.
- <sup>14</sup>A. Chaigne, "Modélisation du piano et couplage cordes-chevalet" ("Modeling of the piano and string-bridge coupling"), in *Proceedings of the 12ème Congrès Français d'Acoustique*, Poitiers, France (April 22–25, 2014), pp. 1085–1091.
- <sup>15</sup>A. Banerjee, A. Chanda, and R. Das, "Historical origin and recent development on normal directional impact models for rigid body contact simulation: A critical review," *Arch. Comput. Methods Eng.* **24**, 397–422 (2017).
- <sup>16</sup>V. Chatziioannou and M. van Walstijn, "Energy conserving schemes for the simulation of musical instrument contact dynamics," *J. Sound Vib.* **339**, 262–279 (2015).
- <sup>17</sup>S. Bilbao, A. Torin, and V. Chatziioannou, "Numerical modeling of collisions in musical instruments," *Acta Acust. united Acust.* **101**(1), 155–173 (2015).
- <sup>18</sup>C. Issanchou, V. Acary, F. Pérignon, C. Touzé, and J.-L. Le Carrou, "Nonsmooth contact dynamics for the numerical simulation of collisions in musical string instruments," *J. Acoust. Soc. Am.* **143**(5), 3195–3205 (2018).
- <sup>19</sup>A. Thorin, X. Boutillon, J. Lozada, and X. Merlhiot, "Non-smooth dynamics for an efficient simulation of the grand piano action," *Meccanica* **52**(11), 2837–2854 (2017).
- <sup>20</sup>J. Antunes, V. Debut, L. Borsoi, X. Delaune, and P. Piteau, "A modal Udwardia–Kalaba formulation for vibro-impact modelling of continuous flexible systems with intermittent contacts," *Procedia Eng.* **199**, 322–329 (2017).
- <sup>21</sup>J. Antunes and V. Debut, "Dynamical computation of constrained flexible systems using a modal Udwardia–Kalaba formulation: Application to musical instruments," *J. Acoust. Soc. Am.* **141**(2), 764–778 (2017).
- <sup>22</sup>V. Debut, J. Antunes, M. Marques, and M. Carvalho, "Physics-based modeling techniques of a twelve-string Portuguese guitar: A non-linear time-domain computational approach for the multiple-strings/bridge/soundboard coupled dynamics," *Appl. Acoust.* **108**, 3–18 (2016).
- <sup>23</sup>V. Debut and J. Antunes, "Physical synthesis of six-string guitar plucks using the Udwardia–Kalaba modal formulation," *J. Acoust. Soc. Am.* **148**(2), 575–587 (2020).
- <sup>24</sup>C. d'Alessandro and B. F. G. Katz, "Tonal quality of the clavichord: The effect of sympathetic strings," in *Proceedings of the International Symposium on Musical Acoustics ISMA '04*, Nara, Japan (March 31–April 3, 2004), pp. 21–24.
- <sup>25</sup>J.-T. Jiolat, C. d'Alessandro, and J.-L. Le Carrou, "L'effet acoustique des cordes mortes du clavicorde ("The acoustic effect of the dead strings of the clavichord"), in *Proceedings of Congrès Français d'Acoustique (CFA 2018)*, Le Havre, France (April 23–27, 2018), pp. 233–239.
- <sup>26</sup>J.-L. Le Carrou, D. Chadeaux, L. Seydoux, and B. Fabre, "A low-cost high-precision measurement method of string motion," *J. Sound Vib.* **333**(17), 3881–3888 (2014).
- <sup>27</sup>R. Roy and T. Kailath, "Esprit-estimation of signal parameters via rotational invariance techniques," *IEEE Trans. Acoust. Speech Signal Process.* **37**(7), 984–995 (1989).
- <sup>28</sup>J.-L. Le Carrou, F. Gautier, and R. Badeau, "Sympathetic string modes in the concert harp," *Acta Acust. united Acust.* **95**(4), 744–752 (2009).
- <sup>29</sup>A. Paté, J.-L. Le Carrou, and B. Fabre, "Predicting the decay time of solid body electric guitar tones," *J. Acoust. Soc. Am.* **135**(5), 3045–3055 (2014).
- <sup>30</sup>A. Paté, "Lutherie de la guitare électrique solid body: Aspects mécaniques et perceptifs" ("Lutherie of the solid body electric guitar: Mechanical and perceptual aspects"), Ph.D. thesis, Paris VI, Paris, 2014.
- <sup>31</sup>A. Arda Ozdemir and S. Gumussoy, "Transfer function estimation in system identification toolbox via vector fitting," *IFAC-PapersOnLine* **50**(1), 6232–6237 (2017).
- <sup>32</sup>J. Woodhouse, "Plucked guitar transients: Comparison of measurements and synthesis," *Acta Acust. united Acust.* **90**(5), 945–965 (2004).
- <sup>33</sup>A. Arabyan and F. Wu, "An improved formulation for constrained mechanical systems," *Multibody Syst. Dyn.* **2**(1), 49–69 (1998).
- <sup>34</sup>G. Kirchhoff, *Vorlesungen Über Mechanik (Lectures on Mechanics)* (BG Teubner, Leipzig, Germany, 1883).
- <sup>35</sup>G. F. Carrier, "On the non-linear vibration problem of the elastic string," *Q. Appl. Math.* **3**(2), 157–165 (1945).
- <sup>36</sup>D. R. Rowland, "The potential energy density in transverse string waves depends critically on longitudinal motion," *Eur. J. Phys.* **32**(6), 1475–1484 (2011).
- <sup>37</sup>C. Cuesta and C. Valette, *Mécanique de la Corde Vibrante (Vibrating String Mechanics)* (Hermès, Paris, 1993), p. 520.
- <sup>38</sup>S. Yoon, R. M. Howe, and D. T. Greenwood, "Geometric elimination of constraint violations in numerical simulation of Lagrangian equations," *J. Mech. Des.* **116**(4), 1058–1064 (1994).
- <sup>39</sup>F. Marques, A. P. Souto, and P. Flores, "On the constraints violation in forward dynamics of multibody systems," *Multibody Syst. Dyn.* **39**(4), 385–419 (2017).
- <sup>40</sup>See <https://www.musimediane.com/numero7/ALESSANDRO/> for viewed high speed video of the string motion in the vicinity of the tangent (Last viewed 9/20/21).
- <sup>41</sup>A. De Cheveigné and H. Kawahara, "Yin, a fundamental frequency estimator for speech and music," *J. Acoust. Soc. Am.* **111**(4), 1917–1930 (2002).
- <sup>42</sup>J.-L. Le Carrou, D. Chadeaux, M.-A. Vitrani, S. Billout, and L. Quartier, "Dropic: A tool for the study of string instruments in playing conditions," in *Proceedings of Acoustics 2012*, Nantes, France (April 23–27, 2012).